CONDENSED MATTER PHYSICS

Proximity effect of emergent field from spin ice in an oxide heterostructure

Mizuki Ohno[1]*†, Takahiro C. Fujita[1]*†, Masashi Kawasaki[1,2]

Geometrical frustration endows magnets with degenerate ground states, resulting in exotic spin structures and quantum phenomena. Such magnets, called quantum magnets, can display non-coplanar spin textures and be a viable platform for the topological Hall effect driven by "emergent field." However, most quantum magnets are insulators, making it challenging to electrically detect associated fluctuations and excitations. Here, we probe magnetic transitions in the spin ice insulator $Dy_2Ti_2O_7$, a prototypical quantum magnet, as emergent magnetotransport phenomena at the heterointerface with the nonmagnetic metal $Bi_2Rh_2O_7$. Angle-dependent longitudinal resistivity exhibits peaks at the magnetic phase boundaries of spin ice due to domain boundary scattering. In addition, the anomalous Hall resistivity undergoes a sign change with the magnetic transition in $Dy_2Ti_2O_7$, reflecting the inversion of the emergent field. These findings, on the basis of epitaxial techniques, connect the fundamental research on insulating quantum magnets to their potential electronic applications, possibly leading to transformative innovations in quantum technologies.

INTRODUCTION

Geometrically frustrated spin systems exhibit an inherent incompatibility between the lattice geometry and the magnetic interactions, resulting in macroscopically degenerate ground-state manifolds (*1*–*4*). The large magnetocrystalline anisotropy and magnetic interactions in these systems give rise to exotic ground states, and field-induced phase transitions in these states lead to emergent quantum phenomena. For example, entanglement fluctuations and quasiparticle excitations equivalent to magnetic monopoles provide the potential toward revolutionary quantum technologies (*5*–*10*). Such materials are referred to as quantum magnets, as represented by "spin-ice" state (*11*–*19*) characterized by its distinctive non-coplanar spin textures. Nevertheless, a considerable obstacle lies in the fact that many quantum magnets are insulating in nature, making it challenging to integrate them into electronic circuits and technologies based on conducting charge carriers. In addition, spin structure and magnetic transition in quantum magnets have been studied only at ultralow temperatures (~0.5 K) by using such techniques as magnetization, neutron scattering, heat capacity, magnetodielectric, capacitive torque magnetometry, and ultrasound (*11*–*26*). Therefore, there is a growing demand to develop a new method for electrically detecting emergent fluctuations and excitations in quantum magnets without disrupting the spin states.

In this study, we demonstrate the electrical detection of the magnetic transition in a quantum magnet by leveraging proximity effect of emergent field for an epitaxial pyrochlore heterostructure consisting of $Bi_2Rh_2O_7/Dy_2Ti_2O_7$ (BRO/DTO), where DTO is an archetypical spin-ice insulator and BRO is a nonmagnetic conductor (Fig. 1, A and B) (*27*, *28*). DTO falls into spin-ice state below 1 K, where the ground state of each tetrahedron settles in one of the sixfold degenerate 2-in-2-out (2/2) configurations that are stabilized because of ferromagnetic interaction and strong magnetic anisotropy along the ⟨111⟩ direction of the pyrochlore lattice (*13*, *14*, *17*, *18*, *29*). A magnetic field (B) along the ⟨111⟩ direction breaks the ice rule and induces the spin flop transition from 2/2 to 3-in-1-out (3/1) configuration (Fig. 1, C and D), giving rise to a jump in magnetization from ~3.3 to ~5 μ_B/Dy between two magnetization plateaus (*15*, *16*). These non-coplanar spin textures have scalar spin chirality, which is proportional to the solid angle subtended by the spins and acts as an "emergent field (b_{em})" for the conducting charge carriers coupled to the spins, resulting in topological Hall effect (*30*–*32*). By constructing a coherent heterointerface with a nonmagnetic metal BRO, we successfully detected sign inversion of b_{em} associated with the spin flop transition in DTO through the topological Hall effect in BRO (Fig. 1B). Furthermore, field-angle dependence of longitudinal resistivity manifests unique peaks at the magnetic phase boundaries of spin-ice state, unambiguously demonstrating the presence of proximity effect on the conducting charges stemming from the spin structure of DTO at the heterointerface. The interfacial approach can be readily extended to other frustrated insulating quantum magnets, facilitating the electrical detection of their exotic spin states and inducing electronic responses (*5*–*10*).

RESULTS

Sample and magnetotransport properties

Epitaxial BRO (111) thin film (9 nm) was grown on DTO layer (60 nm) by pulsed laser deposition (PLD) and subsequent ex situ annealing under O_2 flow (fig. S1, A and B). Relaxed DTO film is prepared by using thin $La_2Zr_2O_7$ (LZO) buffer layer (~3 nm) on Y-stabilized ZrO_2 (YSZ) (111) substrate and subsequent high temperature in situ annealing (fig. S1, C and D). As a result, we obtained DTO film free from epitaxial strain that exhibits magnetic properties similar to those of bulk single crystals (*16*), including a plateau-like behavior appearing in the "kagome-ice" state (figs. S3 and S4). The full width at half maximum of the rocking curves around (444) peaks of BRO (fig. S1E) and DTO (fig. S1F) are both about 0.07°, evidencing the high crystallinity of the films. BRO layer is coherently grown on the DTO layer under tensile strain (fig. S1, G and H). As confirmed in the transmission electron microscopy image (Fig. 1E) and the energy dispersive x-ray spectroscopies (Figs. 1, F to I), the Bi, Rh, Dy, and Ti

[1]Department of Applied Physics and Quantum-Phase Electronics Center (QPEC), University of Tokyo, Tokyo 113-8656, Japan. [2]RIKEN Center for Emergent Matter Science (CEMS), Wako 351-0198, Japan.
*Corresponding author. Email: ohno@kwsk.t.u-tokyo.ac.jp (M.O.); fujita@ap.t.u-tokyo.ac.jp (T.C.F.)
†These authors contributed equally to this work.

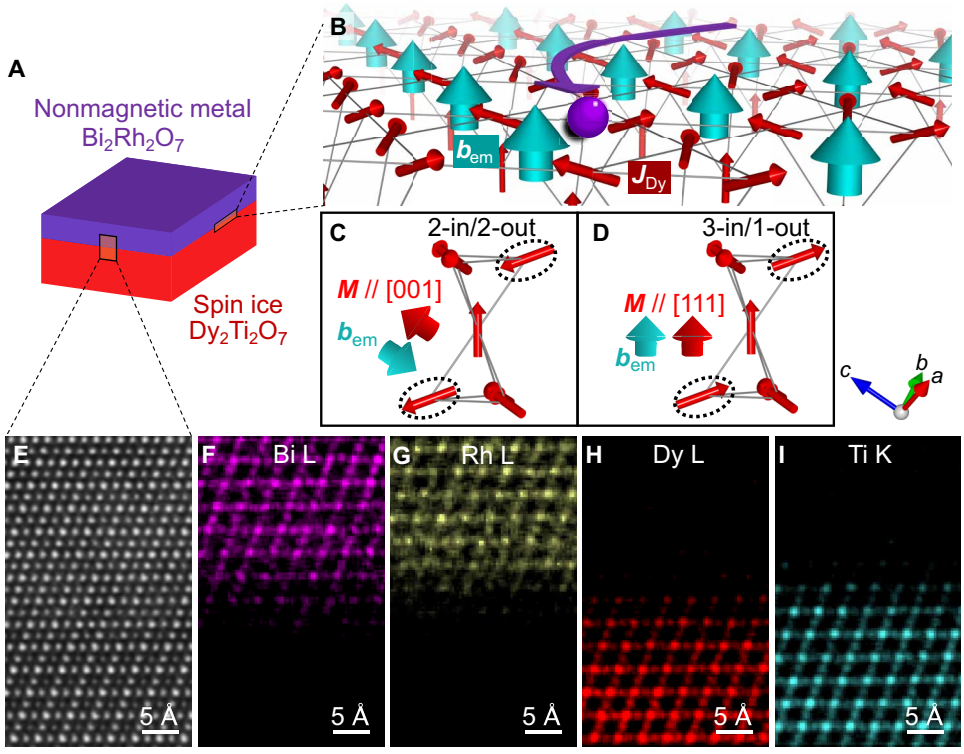

Fig. 1. $Dy_2Ti_2O_7/Bi_2Rh_2O_7$ pyrochlore heterostructure. (**A**) A schematic of the heterostructure composed of nonmagnetic metal $Bi_2Rh_2O_7$ (BRO) and magnetic insulator $Dy_2Ti_2O_7$ (DTO) with spin ice configuration. (**B**) A schematic of the BRO/DTO interface. The charge carrier (purple) on the BRO side flows through the proximitized emergent field b_{em} (green) penetrating from DTO with 3-in/1-out (3/1) configuration of local spins J_{Dy} (red), resulting in the transverse Hall current (curved purple arrow). The net b_{em} and magnetization M in a pair of tetrahedra consisting of Dy spins with (**C**) 2-in/2-out (2/2) and (**D**) 3/1 configurations under magnetic field along [001] and [111] directions. When the magnetic field is rotated from [001] to [111] directions, the spins surrounded by the dotted ellipses in (C) are flopped to those in (D), resulting in a transition from 2/2 to 3/1 configurations. (**E**) High-resolution high-angle annular dark-field scanning transmission electron microscopy (STEM) image of the film. The corresponding energy dispersive x-ray spectrometry maps for (**F**) Bi L, (**G**) Rh L, (**H**) Dy L, and (**I**) Ti K edges.

atoms are periodically arranged to form pyrochlore structure without any discernible crystallographic defects or interdiffusions. Wide range transmission electron microscopy images (fig. S2) further support the presence of sharp interfaces.

Figure 2 summarizes the fundamental magnetotransport properties of the BRO/DTO. To characterize the effect of magnetic order in DTO, we compare the transport properties of BRO film on nonmagnetic $Eu_2Ti_2O_7$ (ETO), where BRO exhibits intrinsic transport properties (figs. S5 and S6). The electrical properties of BRO/ETO resemble those of nonmagnetic dirty metals, with almost temperature independent longitudinal resistivity (ρ_{xx}), positive magnetoresistance (MR) up to ~1.6% at 2 K, and linear Hall resistivity (ρ_{yx}) with a positive slope (fig. S6). As shown in Fig. 2A, BRO/DTO shows similar temperature dependence of ρ_{xx} at higher temperatures above ~30 K under $B = 0$ or 9 T. In contrast, it shows a larger upturn below 30 K in BRO/DTO than in BRO/ETO. This difference is also confirmed by MR ratio [$\equiv \rho_{xx}(B)/\rho_{xx}(0) - 1$], where positive MR of BRO is suppressed below 50 K as shown in Fig. 2B. In particular, at 2 K, negative MR is observed at low fields. This can be explained by considering both intrinsic positive MR of BRO and magnetic scattering at the interface from DTO as discussed in the following. Figure 2C presents ρ_{yx} of BRO/DTO measured at various temperatures. Above 50 K, ρ_{yx} depends almost linearly on the magnetic field, similar to nonmagnetic BRO/ETO (fig. S6). In stark contrast, it deviates from the linear behavior upon cooling below 50 K, suggesting the contribution of magnetic order in DTO. Empirically, ρ_{yx} is expressed as $\rho_{yx} = R_H B + \rho_{AHE}$ with the ordinary Hall coefficient R_H and the anomalous Hall resistivity ρ_{AHE}. By subtracting the ordinary Hall term with a linear fit between 7 and 9 T, ρ_{AHE} is obtained as shown in Fig. 2D. Unexpectedly, at 2 K, ρ_{AHE} exhibits a sign inversion, which cannot be explained only by a conventional anomalous Hall component proportional to magnetization [$\alpha M_{[111]}$]. Here, α is a constant independent of magnetic field and temperature (see Supplementary Text for the definition of α more in details). These results strongly indicate that the magnetic ordering of DTO and the conducting charge carriers in BRO are tightly coupled, exerting a profound influence on both ρ_{xx} and ρ_{yx}. To further explore this relationship, we have performed in-depth analyses of the magnetic field-angle dependence of ρ_{xx} and the characteristics of ρ_{AHE} to shed light on the evident connection between the spin-ice configurations of DTO and the observed emergent transport phenomena.

Field-angle dependence of longitudinal resistivity

To confirm the transport modification of BRO related to the spin configurations of DTO, we have investigated field-angle dependence of ρ_{xx} as shown in Fig. 3. The origin of the rotation angle ($\theta = 0°$) is defined to be the B // [111] direction, and the field is rotated around the [1$\bar{1}$0] axis parallel to the current (I) direction (Fig. 3A), passing

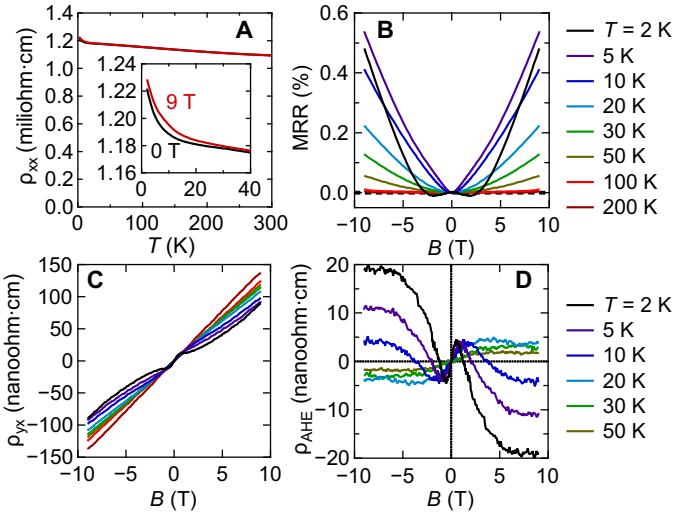

Fig. 2. Magnetotransport properties. (**A**) Temperature dependence of ρ_{xx} for the BRO (9 nm) thin film on DTO under $B = 0$ T (black) and 9 T (red) applied along the [111] direction. The inset shows an enlarged view at low temperatures. Magnetic field (B) dependence of (**B**) MR ratio [MRR $\equiv \rho_{xx}(B)/\rho_{xx}(0) - 1$] and (**C**) Hall resistivity (ρ_{yx}) measured at various temperatures. (**D**) Anomalous Hall resistivity ρ_{AHE} obtained by subtracting the ordinary Hall term.

through the [001] axis at θ = 55°, the $[\bar{1}\,\bar{1}\,2]$ axis at θ = 90°, the $[\bar{1}\,\bar{1}\,0]$ axis at θ = 145°, and lastly the $[\bar{1}\,\bar{1}\,\bar{1}]$ axis at θ = 180°. Figure 3C presents angle-dependent magnetoresistance ratio [ADMR $\equiv \rho_{xx}(\theta)/\rho_{xx}(0°) - 1$] measured at various temperatures with a fixed magnetic field of 9 T, where unique peak structures appear at θ = 19°, 90°, and 145° below 20 K. Considering that the peaks become smaller with increasing temperature, this field-angle dependence can be attributed to the change in magnetic ordering of DTO, which is further verified by the fact that isotropic transport is indeed observed in BRO/ETO (fig. S7).

To elucidate the origin of observed angle dependence, we have considered field-angle–dependent spin configurations of DTO based on a simple assumption: Four distinct types of spin in a pair of tetrahedra, denoted by Dy i (i = 1 to 4) in the top of Fig. 3D, are always aligned along the applied field to gain Zeeman energy ($\mathbf{M}\cdot\mathbf{B} > 0$) under high-field limit. Under this assumption, 3/1 state is realized at θ = 0° (B // [111]). With rotating the field angle, Dy2 is flopped at θ = 19° and 2/2 state is realized. Similarly, Dy1 (Dy3 and Dy4) is (are) flopped at θ = 90° (145°) and 3/1 [1-in/3-out (1/3)] state is realized. In our heterostructure, at higher temperatures above 30 K, a conventional anisotropic ADMR originating from the magnetizations of DTO is dominant and follows |sinθ| dependence exhibiting a maximum value at θ = 90°. In the low-temperature region, in addition to the conventional ADMR, additional contribution of comparable magnitude is visible at 145° (B // $[\bar{1}\,\bar{1}\,0]$), reflecting those two spins (Dy3 and Dy4) flop at the boundary between 3/1 and 1/3 states. Identical pattern is repeated in the region of 180° to 360°, suggesting the 180° periodicity which is indeed expected for the spin-ice state. Considering the above spin configuration of DTO, the observed peaks in ADMR correspond to the magnetic phase boundaries between 2/2, 3/1, and 1/3 states. The spins adjacent to these boundaries are unstable and fluctuating and thus impose more scattering on the conducting charge carriers that increases the resistivity. At 2 K, almost same field-angle dependence except for the overall magnitude is observed above 3 T (fig. S8), suggesting that 9 T is strong enough to realize the angle-dependent spin configuration of DTO under high-field limit. These results clearly demonstrate that

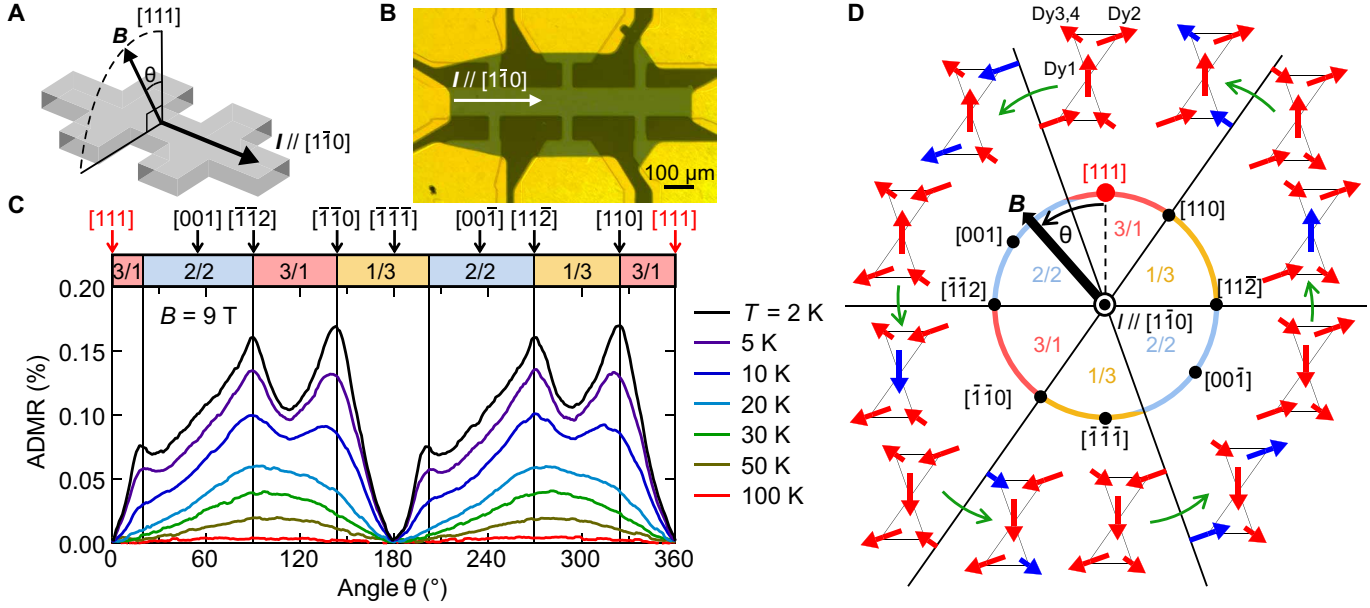

Fig. 3. Scattering at the magnetic phase boundaries. (**A**) A schematic of measurement configuration. The field angle θ is defined from the surface normal [111] direction. (**B**) A top-view photograph of the measured Hall bar device structure with a channel width of 100 μm. (**C**) The top denotes the corresponding crystallographic directions and expected magnetic structures of the Dy 4*f* moments under high-field limit: 2/2, 3/1, and 1/3 represent "2-in/2-out," "3-in/1-out," and "1-in/3-out" configurations, respectively. The bottom shows the ADMR [ADMR $\equiv \rho_{xx}(\theta)/\rho_{xx}(0°) - 1$] for several temperatures at 9 T. (**D**) Schematic spin configurations while rotating magnetic field. Blue arrows represent flopped spins across the boundary in spin structures (black lines). Four distinct types of spin in a pair of tetrahedra are denoted as "Dy1," "Dy2," "Dy3," and "Dy4."

the spin configuration of spin-ice state is detected through ADMR at the present BRO/DTO heterointerface.

Topological Hall effect

Having clarified the unique ADMR related to the spin configuration of DTO, we proceed to delve into the topological Hall effect that is, to the best of our knowledge, the first observation induced by the proximity effect of emergent field (b_{em}). The sign inversion in ρ_{AHE} seen in Fig. 2D can be consistently explained by considering the topological Hall effect resulting from b_{em} associated with non-coplanar spin configurations inherent in the spin-ice state. At a tetrahedron, b_{em} is antiparallel to the magnetization in 2/2 configuration (Fig. 4B), whereas it is parallel to the magnetization in 3/1 configuration (Fig. 4C). This enables a manipulation of b_{em} through the application of an external magnetic field along the [111] direction during the domain alignment process (Fig. 4A), concomitant with the sign inversion triggered by the spin flop transition. First, b_{em} are canceled out in the ground state of sixfold degenerate 2/2 configurations (2/2{6}) at 0 T. By applying magnetic field along the [111] direction, 2/2{6} state is gradually lifted to the threefold degenerate 2/2 states, leading to the fully aligned kagome-ice state (2/2{3}) at ~1 T, which is followed by the ferromagnetic 3/1 state (3/1{1}) at ~2 T. During this process, b_{em} grows with antiparallel to magnetization below ~1 T, the average of which ($b_{em,ave}$) is antiparallel to the [111] direction as shown in Fig. 4A(b). Then, $b_{em,ave}$ is flipped from antiparallel to parallel to the [111] direction toward 3/1{1} state shown in Fig. 4A(c).

The observed ρ_{AHE} at low temperatures (Fig. 4D) can be straightforwardly understood as a summation of the conventional anomalous Hall term proportional to magnetization ($\alpha M_{[111]}$) and the topological Hall term (ρ_{THE}) due to $b_{em,ave}$ accompanied with a sign inversion

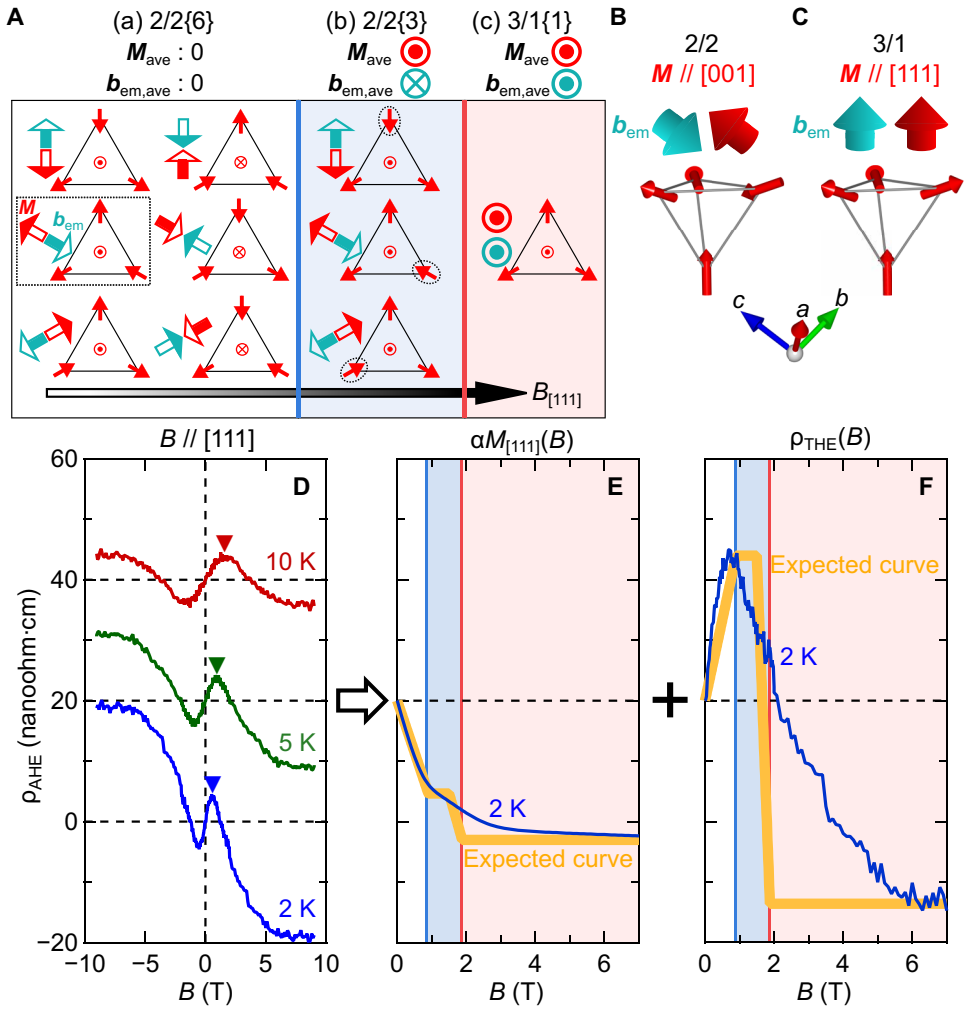

Fig. 4. Topological Hall effect. (**A**) The degeneracy lifting process of spin ice when magnetic field is increased along the out-of-plane [111] direction: (a) Sixfold degenerate 2/2 states (2/2{6}) at $B = 0$ T, (b) threefold degenerate 2/2 states (2/2{3}) under intermediate field, and (c) nondegenerate 3/1 state (3/1{1}) under high-field limit. Top-view schematic spin configurations are illustrated for each state, with net M and b_{em} in a tetrahedron represented as red and green arrows, respectively. When the out-of-plane component is parallel (antiparallel) to the [111] direction, arrowhead is filled (open). M_{ave} ($b_{em,ave}$) stands for the average of M (b_{em}) defined as the summation of M (b_{em}) among the degenerate configurations in each state, which is (a) zero (zero), (b) parallel (antiparallel), (c) parallel (parallel) to the [111] direction. Three-dimensional schematics for the net M and b_{em} components in a tetrahedron with (**B**) 2/2 [surrounded by dotted lines in (A)] and (**C**) 3/1 configurations. (**D**) Anomalous Hall resistivity ρ_{AHE} measured at 2, 5, and 10 K under B // [111], where the peak of ρ_{AHE} is marked by the triangles. In particular, ρ_{AHE} at 2 K is deconvoluted into (**E**) $\alpha M_{111}(B)$ and (**F**) ρ_{THE} with assuming $\alpha = 0.4 \times \rho_{AHE}(7\,T)/M_{111}(7\,T)$. The magnetization curve of DTO film under 7 T [fig. S4(a)] is used for $M_{111}(B)$. Background colors correspond to three states in (A). The boundaries of the three states are determined on the basis of an expected signal (yellow) at 0 K.

as shown with blue curves in Fig. 4 (E and F), respectively (see Supplementary Text and fig. S10 for the analysis of ρ_{AHE} in more details). Note that the yellow schematic signals are indicated for clear magnetic transition processes without thermal fluctuation following the scenario discussed above. Furthermore, we found that such sign inversion in ρ_{AHE} is absent when the magnetic field is along the [001] direction, where the spin flop transition to the 3/1 state does not take place (fig. S9) (*15*). These results confirm that the sign inversion in ρ_{AHE} is indeed attributed to the transition from 2/2 to 3/1 states under the magnetic field along the [111] direction. Another intriguing feature of ρ_{AHE} is its temperature dependence shown in Fig. 2D. In DTO, magnetic anisotropy along the ⟨111⟩ direction and the nearest-neighbor interaction, both of which construct the spin ice ground state at low temperatures, remain up to ~70 K (*12*, *14*, *18*, *22*). This suggests that thermally fluctuated spins favor 2/2 like spin configurations rather than 3/1 even at high temperatures. Upon increasing temperature, the anomalous Hall term proportional to magnetization is expected to decrease following the magnetization curve. In contrast, the topological Hall term is anticipated to undergo substantial changes in profile, with the positive component from 2/2 state becoming dominant. In our heterostructure, with increasing the temperature from 2 to 10 K, the peak of ρ_{AHE} becomes broader and shifts toward higher fields, indicating that 2/2 like spin configuration is expanded due to the thermal fluctuation. At 20 K, the contribution from the 2/2 state becomes dominant, resulting in the absence of negative topological Hall resistivity. With further increase in temperature, the topological component becomes smaller and eventually undetectable at 100 K (Fig. 2D).

DISCUSSION

In summary, we have demonstrated the intriguing magnetotransport properties in an epitaxial pyrochlore oxide heterostructure consisting of nonmagnetic metal BRO and spin ice insulator DTO. We observe the angle-dependent MR that is consistent with the magnetic phase transition in the spin ice state of DTO. We also identify the topological Hall resistivity as an evidence for the sign inversion of an emergent field triggered by the spin flop transition. This observation suggests that the magnetic proximity effect not only induces the anomalous Hall effect proportional to magnetization but also promotes the topological Hall effect through the "penetration" of the emergent field. These results demonstrate that epitaxial heterostructures are highly promising platforms to investigate interactions between localized frustrated spins and conducting charge carriers. This approach opens the possibilities for electronically probing charge conversion of the monopole condensation excitations under non-equilibrium stimuli (*5*, *7*, *33*, *34*). Recent proposals have suggested the existence of a two-dimensional monopole gas at the heterointerface of the 2-in-2-out and the all-in-all-out states (*35*). Such behavior may manifest itself in electronic transport phenomena when coupled with charge carriers, offering an alternative detection method and a potential pathway for practical applications. Therefore, our work paves a way toward further exploration and functionalization of quantum magnets through the interface-induced emergent transport phenomena.

MATERIALS AND METHODS

Thin-film growth

The BRO/DTO/LZO (111) thin film was grown on YSZ (111) substrates by PLD and subsequent ex situ annealing (fig. S1A). Thickness of the BRO layer on DTO is 9 nm. One identical sample is used for all the transport and structural measurements in this work. PLD targets of BRO, DTO, and LZO were prepared by a solid state reaction (*27*, *36*–*39*). KrF excimer laser pulses ($\lambda = 248$ nm) were used to ablate the targets, with a fluence and frequency of 1 J/cm^2 and 5 Hz. The LZO and DTO layers were deposited at 850°C under 1×10^{-4} torr O_2 and subsequently in situ annealed at 1100°C for 10 min. Amorphous precursor Bi-Rh-O layer was then deposited at room temperature under 5×10^{-7} torr O_2, with the pure BRO phase appearing after annealing in a tube furnace at 1000°C for 1 hour under O_2 flow.

Device fabrication and magnetotransport measurements

The Hall bar structure was processed by conventional photolithography and Ar ion milling. Ohmic Ni (10 nm)/Au (50 nm) contacts were deposited by an electron-beam evaporator, as shown in Fig. 2B. Magnetotransport measurements were performed in a liquid He cryostat equipped with a 9 T superconducting magnet (Physical Properties Measurement System, Quantum Design Co.).

Magnetic measurements

Magnetic measurements for the DTO film were performed with a superconducting quantum interference device magnetometer (MPMS3, Quantum Design Co.) down to 2 K and up to 7 T.

Supplementary Materials

This PDF file includes:

Supplementary Text
Figs. S1 to S10
References

REFERENCES AND NOTES

1. C. Lacroix, P. Mendels, F. Mila, Ed., *Introduction to Frustrated Magnetism* (Springer Berlin, 2011).
2. H. T. Diep, Ed., *Frustrated Spin Systems* (World Scientific, Singapore, ed. 2, 2013).
3. A. P. Ramirez, Strongly geometrically frustrated magnets. *Annu. Rev. Mater. Sci.* **24**, 453–480 (1994).
4. J. S. Gardner, M. J. Gingras, J. E. Greedan, Magnetic pyrochlore oxides. *Rev. Mod. Phys.* **82**, 53 (2010).
5. C. Castelnovo, R. Moessner, S. L. Sondhi, Magnetic monopoles in spin ice. *Nature* **451**, 42–45 (2008).
6. L. Balents, Spin liquids in frustrated magnets. *Nature* **464**, 199–208 (2010).
7. D. I. Khomskii, Electric dipoles on magnetic monopoles in spin ice. *Nat. Commun.* **3**, 904 (2012).
8. L. Savary, L. Balents, Quantum spin liquids: A review. *Rep. Prog. Phys.* **80**, 016502 (2017).
9. Y. Zhou, K. Kanoda, T.-K. Ng, Quantum spin liquid states. *Rev. Mod. Phys.* **89**, 025003 (2017).
10. G. Semeghini, H. Levine, A. Keesling, S. Ebadi, T. T. Wang, D. Bluvstein, R. Verresen, H. Pichler, M. Kalinowski, R. Samajdar, A. Omran, S. Sachdev, A. Vishwanath, M. Greiner, V. Vuletić, M. D. Lukin, Probing topological spin liquids on a programmable quantum simulator. *Science* **374**, 1242–1247 (2021).
11. M. J. Harris, S. T. Bramwell, D. F. McMorrow, T. Zeiske, K. W. Godfrey, Geometrical frustration in the ferromagnetic Pyrochlore $Ho_2Ti_2O_7$. *Phys. Rev. Lett.* **79**, 2554–2557 (1997).
12. S. T. Bramwell, M. N. Field, M. J. Harris, I. P. Parkin, Bulk magnetization of the heavy rare earth titanate pyrochlores—A series of model frustrated magnets. *J. Phys. Condens. Matter* **12**, 483–495 (2000).
13. S. T. Bramwell, M. J. Harris, B. C. den Hertog, M. J. P. Gingras, J. S. Gardner, D. F. McMorrow, A. R. Wildes, A. L. Cornelius, J. D. M. Champion, R. G. Melko, T. Fennell, Spin correlations in $Ho_2Ti_2O_7$: A dipolar spin ice system. *Phys. Rev. Lett.* **87**, 047205 (2001).
14. Y. M. Jana, A. Sengupta, D. Ghosh, Estimation of single ion anisotropy in pyrochlore $Dy_2Ti_2O_7$, a geometrically frustrated system, using crystal field theory. *J. Magn. Magn. Mater.* **248**, 7–18 (2002).
15. H. Fukazawa, R. G. Melko, R. Higashinaka, Y. Maeno, M. J. Gingras, Magnetic anisotropy of the spin-ice compound $Dy_2Ti_2O_7$. *Phys. Rev. B* **65**, 054410 (2002).

16. T. Sakakibara, T. Tayama, Z. Hiroi, K. Matsuhira, S. Takagi, Observation of a liquid gas-type transition in the pyrochlore spin ice compound $Dy_2Ti_2O_7$ in a magnetic field. *Phys. Rev. Lett.* **90**, 207205 (2003).
17. R. G. Melko, M. J. Gingras, Monte Carlo studies of the dipolar spin ice model. *J. Phys. Condens. Matter* **16**, R1277 (2004).
18. J. Lago, S. J. Blundell, C., μsR investigation of spin dynamics in the spin-ice material $Dy_2Ti_2O_7$. *J. Phys. Condens. Matter* **19**, 326210 (2007).
19. S. T. Bramwell, M. J. Harris, The history of spin ice. *J. Condens. Matter Phys.* **32**, 374010 (2020).
20. A. Petrenko, R. Lees, G. Balakrishnan, Magnetization process in the spin-ice compound $Ho_2Ti_2O_7$. *Phys. Rev. B* **68**, 012406 (2003).
21. H. Sato, K. Matsuhira, T. Sakakibara, T. Tayama, Z. Hiroi, S. Takagi, Field-angle dependence of the ice-rule breaking spin-flip transition in $Dy_2Ti_2O_7$. *J. Condens. Matter Phys.* **19**, 145272 (2007).
22. S. T. Bramwell, M. J. Gingras, Spin ice state in frustrated magnetic pyrochlore materials. *Science* **294**, 1495–1501 (2001).
23. J. P. C. Ruff, R. G. Melko, M. J. P. Gingras, Finite-temperature transitions in dipolar spin ice in a large magnetic field. *Phys. Rev. Lett.* **95**, 097202 (2005).
24. M. Saito, R. Higashinaka, Y. Maeno, Magnetodielectric response of the spin-ice $Dy_2Ti_2O_7$. *Phys. Rev. B* **72**, 144422 (2005).
25. N. Anand, K. Barry, J. N. Neu, D. E. Graf, Q. Huang, H. Zhou, T. Siegrist, H. J. Changlani, C. Beekman, Investigation of the monopole magneto-chemical potential in spin ices using capacitive torque magnetometry. *Nat. Commun.* **13**, 3818 (2022).
26. S. Erfanifam, S. Zherlitsyn, S. Yasin, Y. Skourski, J. Wosnitza, A. A. Zvyagin, P. McClarty, R. Moessner, G. Balakrishnan, O. A. Petrenko, Ultrasonic investigations of the spin icesDy$_2$Ti$_2$O$_7$ and $Ho_2Ti_2O_7$ in and out of equilibrium. *Phys. Rev. B* **90**, 064409 (2014).
27. J. M. Longo, P. M. Raccah, J. A. Kafalas, J. W. Pierce, Preparation and structure of a pyrochlore and perovskite in the $BiRhO_{3+}x$ system. *Mat. Res. Bull.* **7**, 137–146 (1972).
28. M. Ohno, T. C. Fujita, M. Kawasaki, Impact of iso-structural template layer on stabilizing pyrochlore $Bi_2Rh_2O_7$. *Appl. Phys. Lett.* **122**, 251601 (2023).
29. A. P. Ramirez, A. Hayashi, R. J. Cava, R. Siddharthan, B. S. Shastry, Zero-point entropy in 'spin ice'. *Nature* **399**, 333–335 (1999).
30. J. Ye, Y. B. Kim, A. J. Millis, B. I. Shraiman, P. Majumdar, Z. Tešanović, Berry phase theory of the anomalous hall effect: Application to colossal magnetoresistance manganites. *Phys. Rev. Lett.* **83**, 3737–3740 (1999).
31. K. Ohgushi, S. Murakami, N. Nagaosa, Spin anisotropy and quantum Hall effect in thekagomélattice: Chiral spin state based on a ferromagnet. *Phys. Rev. B* **62**, R6065–R6068 (2000).
32. N. Nagaosa, Anomalous hall effect—A new perspective. *J. Physical Soc. Japan* **75**, 042001 (2006).
33. E. Lhotel, L. D. Jaubert, P. C. Holdsworth, Fragmentation in frustrated magnets: A review. *J. Low Temp. Phys.* **201**, 710–737 (2020).
34. C. Paulsen, M. J. Jackson, E. Lhotel, B. Canals, D. Prabhakaran, K. Matsuhira, S. R. Giblin, S. T. Bramwell, Far-from-equilibrium monopole dynamics in spin ice. *Nat. Phys.* **10**, 135–139 (2014).
35. L. Miao, Y. Lee, A. B. Mei, M. J. Lawler, K. M. Shen, Two-dimensional magnetic monopole gas in an oxide heterostructure. *Nat. Commun.* **11**, 1341 (2020).
36. B. J. Kennedy, Structural trends in Bi containing pyrochlores: The structure of $Bi_2Rh_2O_{7-\delta}$. *Mat. Res. Bull.* **32**, 479–483 (1997).
37. X. Li, Q. Q. Liu, W. Han, Y. Liu, X. D. Li, Y. C. Li, J. Liu, C. Q. Jin, Synthesis and structural stability of $BiRhO_3$ at high pressure. *Int. J. Mod. Phys* **27**, 1362021 (2013).
38. A. Bayart, J.-F. Blach, M. Huvé, F. Blanchard, P. Roussel, R. Desfeux, S. Saitzek, Optical properties of $Ln_2Ti_2O_7$ (with Ln = La to Lu) thin films grown on (110)-$SrTiO_3$ substrates by pulsed laser deposition. *Opt. Mater.* **92**, 303–310 (2019).
39. A. Panghal, P. K. Kulriya, Y. Kumar, F. Singh, N. L. Singh, Investigations of atomic disorder and grain growth kinetics in polycrystalline $La_2Zr_2O_7$. *Appl. Phys. A* **125**, 428 (2019).
40. K. Terai, M. Lippmaa, P. Ahmet, T. Chikyow, T. Fujii, H. Koinuma, M. Kawasaki, In-plane lattice constant tuning of an oxide substrate with $Ba_{1-}xSr_xTiO_3$ and $BaTiO_3$ buffer layers. *Appl. Phys. Lett.* **80**, 4437–4439 (2002).
41. V. Lazarev, I. Shaplygin, Electrical properties of mixed oxides containing a platinum metal and a non-noble metal. *Russ. J. Inorg. Chem.* **23**, 163–169 (1978).
42. A. M. Hallas, A. Z. Sharma, C. Mauws, Q. Chen, H. D. Zhou, C. Ding, Z. Gong, M. Tachibana, P. M. Sarte, J. P. Attfield, G. M. Luke, C. R. Wiebe, Coexistence of metallic and nonmetallic properties in the pyrochlore $Lu_2Rh_2O_7$. *npj Quantum Mater.* **4**, 9 (2019).

Acknowledgments: We thank N. Nagaosa for fruitful discussions. The magnetic measurements were performed using the facilities of the Cryogenic Research Center, the University of Tokyo. **Funding:** This work was supported by JSPS Grants-in-Aid for Scientific Research (S) no. JP22H04958 (M.K.), JSPS Grant-in-Aid for Early-Career Scientists no. JP20K1516 (T.C.F.), JSPS Fellowship no. JP22J12905 (M.O.), Mitsubishi Foundation (M.K.), The Murata Science Foundation (T.C.F.), Mizuho Foundation for the Promotion of Sciences (T.C.F.), Iketani Science and Technology Foundation (T.C.F.), Kazuchika Okura Memorial Foundation (T.C.F.), and Yazaki Memorial Foundation for Science and Technology (T.C.F.). **Author contributions:** Conceptualization: T.C.F. and M.K. Methodology: M.O., T.C.F., and M.K. Investigation: M.O. and T.C.F. Visualization: M.O. and T.C.F. Supervision: T.C.F. and M.K. Writing—original draft: M.O. and T.C.F. Writing—review and editing: T.C.F. and M.K. Funding acquisition: M.O., T.C.F., and MK. Project administration: T.C.F. and M.K. Validation: M.O., T.C.F., and M.K. **Competing interests:** The authors declare that they have no competing interests. **Data and materials availability:** All data needed to evaluate the conclusions in the paper are present in the paper and/or the Supplementary Materials.

Submitted 1 September 2023
Accepted 6 February 2024
Published 13 March 2024
10.1126/sciadv.adk6308